Temperature and Salinity Variability in the Deep Western Boundary Current

SHARI L. VAUGHAN

Prince William Sound Science Center, Cordova, Alaska

ROBERT L. MOLINARI

National Oceanic and Atmospheric Administration, Atlantic Oceanographic and Meteorological Laboratory, Miami, Florida

(Manuscript received 12 September 1995, in final form 9 October 1996)

ABSTRACT

A ten-year time series (1984–1993) of repeat hydrographic sections from offshore Abaco Island, the Bahamas (26.5°N), is used to define the mean and time dependent characteristics of the deep western boundary current (DWBC). The DWBC flow is divided into four vertical layers based on chlorofluorocarbon (CFC) concentration and formation regions (upper layer: CFC core, $\theta \sim 3.9°$–$5.0°$C; second layer: classical Labrador Sea Water, $\theta \sim 3.2°$–$3.9°$C; third layer: CFC minimum, $\theta \sim 2.4°$–$3.2°$C; deepest layer: CFC core, $\theta \sim 1.85°$–$2.4°$C). Time series analysis of mean layer properties and their anomalies showed that the temperature and salinity of each layer did not increase or decrease monotonically with time. Variations in temperature and salinity were characterized by 2–3-yr period oscillations. Variability between years is illustrated by subtracting repeat sections of temperature and salinity along levels of both constant pressure and constant potential density. To determine an original water mass modification that could be responsible for the observed variability in the section differences, an analytical method, which uses both types of differencing schemes, was applied to the DWBC data. Variability in the upper layer between 1987 and 1993 was shown to originate primarily from an increased salinity of the source waters for this layer. Variability in the second layer was shown to arise from a combination of cooling and salinification. Variability in the two deepest layers seemed to be almost entirely due to vertical movement of the isopycnals. Increases in potential temperature and salinity observed in a sublayer of the second layer defined by $\sigma_{1.5} \sim 34.68$–34.74 (classical Labrador Sea Water) from 1991 to 1993 was shown to be mainly the result of cooling. It is suggested that this cooling may have originally occurred in the central Labrador Sea during the period of active deep water renewal in the early 1970s.

1. Introduction

Several recent studies have provided evidence of long-term, large-scale warming in the intermediate and deep subtropical Atlantic. Roemmich and Wunsch (1984) compared repeat transatlantic sections occupied along 24°N and 36°N during 1957 and 1981. They observed considerable warming [O(0.1°C)] above about 3000 m over the 24-year interval. Parrilla et al. (1994) performed a similar comparison using the 1957 and 1981 occupations and a 1992 reoccupation of the 24°N transect. They concluded that the waters between 800 and 2500 m warmed during the 1957–92 time period. However, between 1981 and 1992, Parrilla et al. (1994, hereafter P94) observed cooling [O(0.05°C)] in the western part of the 24°N section (west of 60°W) and warming in the east.

Since conclusions in both studies were based on differences between sections widely separated in time, the exact timescale of temperature increase is not resolved (Roemmich and Wunsch 1984). The warming could be part of a continuous long-term trend (i.e., periods greater than 35 years) associated with some change in the thermohaline circulation or could result from a shorter term oscillation (i.e., periods less than 35 years) in the deep ocean temperature structure. A ten-year time series (1984–1993) of repeat western boundary hydrographic sections was obtained east of Great Abaco Island, the Bahamas, at 26.5°N (i.e., somewhat to the north of the canonical 24°N transect). The sections provide relatively dense temporal and spatial resolution to consider the question of the timescales of the variability observed by P94 along 24°N.

The 26.5°N sections traverse the velocity core of the deep western boundary current (DWBC), which in this region flows southward between about 1000 m and the bottom (≥4500 m) and typically extends from the shelf break to about 100 km offshore. The DWBC is comprised of water masses originating in the high latitude convection regions and water masses from the interior North Atlantic (e.g., McCartney 1992; Fine 1995). It has long been recognized as the main conduit for trans-

Corresponding author address: Dr. Shari L. Vaughan, Prince William Sound Science Center, P.O. Box 705, Cordova, AK 99574.
E-mail: vaughan@grizzly.pwssc.ger.ak.us

porting recently convected waters away from the northern source regions to the subtropical and tropical North Atlantic. For example, Fine and Molinari (1988), Pickart et al. (1989), Molinari et al. (1992), and Fine (1995) used chlorofluorocarbon observations to demonstrate the continuity of the DWBC.

In the present study, the ten-year time series of hydrographic data off Abaco will be used to accomplish two goals:

1) define the mean temperature and salinity properties of the DWBC and estimate timescales and magnitudes of its variability;
2) determine the type of changes in temperature and salinity structure responsible for the variability between pairs of sections.

The first goal is addressed in section 3 with mean properties described in 3a and variability in section 3b. Transect differences by depth and density are shown in section 4. A method developed by Bindoff and McDougall (1994) is used in section 4a to reconcile the dissimilarities between the two methods of differencing sections and to meet the second goal. Finally, the implications of these results to earlier findings are discussed in section 5.

TABLE 1. Cruise summary including type of data used to calibrate the CTD data (B—bottle, H—historical) and the temperature sensor error given as the average difference between pre- and postcruise laboratory calibrations.

Cruise	Number of stations	Calibration	Maximum eastern extent (°W)	Temperature sensor error (°C)	Maximum depth (dbar)	Number of casts in geost. core by layer
Aug84	6	B	76.0	.002	2010	0/0/0/0
Apr85	10	H	76.3	.003	4130	6/6/4/0
Aug85	6	B	76.3	.001	4100	5/5/5/0
Jan86	11	B, H	76.1	.001	4880	6/6/6/5
Mar86	13	B	75.9	.001	4770	8/8/5/3
Jul86	8	B	75.9	.005	4800	5/5/5/4
Oct86	16	H	75.5	.005	4800	7/7/7/7
Mar87	17	B	74.0	.004	4870	5/5/5/3
Sep87	9	B	75.0	.004	4780	5/5/5/0
Mar88	1	B	75.5	.002	3300	0/0/0/0
Sep88	6	H	76.1	.002	4780	5/5/5/3
Feb89	15	H	74.5	.002	4800	5/5/5/3
Jan90	5	B	75.9	.005	4900	3/3/2/2
Jun90	14	B	71.0	.001	4900	6/6/6/5
Sep90	3	B	74.2	.001	4600	0/0/0/0
Jan91	9	B	75.5	.003	4900	4/4/4/4
Jun91	6	H	74.2	.002	4700	3/3/3/2
Sep91	7	B	73.1	.002	4900	3/3/3/2
Aug92	15	B	70.0	.001	5500	3/3/3/2
Jun93	8	B	71.6	.003	5400	4/4/4/3

2. Data and analysis

The ten-year time series is comprised of hydrographic data collected from August 1984 to June 1993 during 20 cruises (Table 1) along 26.5°N (Fig. 1). The offshore extension of the section varied from 100 to 600 km. Station spacing also varied over the 10-yr period. Cruises earlier than 1986 and some later cruises were limited to about 100 km offshore (76°W), based on the average location of the core of the DWBC during the early stages of the program (Rosenfeld et al. 1989; Lee et al. 1990). In these cruises, the station spacing within the DWBC was of the order 10 km. Later cruises extended farther offshore as it became evident that the core of the DWBC migrated east of 76°W. Within the DWBC, station spacing during these cruises was of the order 20 km. The majority of casts in all but four cruises reached the bottom.

The CTD data were processed by methods given in Wilburn et al. (1987, 1988, 1989) and Johns and Wilburn (1993a,b). Temperature data were examined further by reviewing pre- and postcruise laboratory calibrations of the temperature sensor for evidence of drift. For cruises after 1988, drift was of the order .002°C (Table 1). The largest drifts, .005°C, occurred during several cruises and will serve as a measure of the overall accuracy of the temperature data. Water samples were collected on all cruises and analyzed to provide the salinity data needed to calibrate the CTD sensors. On a few cruises, the calibration data were not adequate and historical data were used to calibrate the CTD salinity sensors. These cruises are noted in Table 1. Comparing calibrated CTD salinities and in situ salinity values indicates that on the average salinities are accurate over the length of the experiment to about .004 psu.

Because of the nonuniform station spacing, contour plots were generated by first interpolating onto finite element grids (extending from 77°W to 74°W and the surface to 4500 m). For example, sections of temperature, salinity, and potential density with pressure as the vertical coordinate were interpolated onto a grid with 21 horizontal and 61 vertical points (i.e., approximately 15-km horizontal and 55-m vertical spacing). Sections were also constructed using potential density referenced to 2000 db (σ_2) as the vertical coordinate. A 21 $\times$ 61 grid was used, which translates to a vertical resolution of .006 in σ_2 and a horizontal resolution of 15 km in longitude. After gridding the synoptic cruise sections, average and standard deviation values were generated at each grid point. A commercial software package routine was then used to contour the synoptic and average sections.

Direct velocity observations indicate that when the core of the DWBC is within 100 km of the boundary, a level of no motion exists at about 800 m (Rosenfeld et al. 1989; Lee et al. 1996). Thus, individual geostrophic velocity sections were referenced to 800 m. As above, synoptic sections were interpolated onto a 21 $\times$ 61 grid and mean sections were generated by averaging the gridded transects.

The average vertical sections all suffer from a similar shortcoming: the number of casts contributing to the

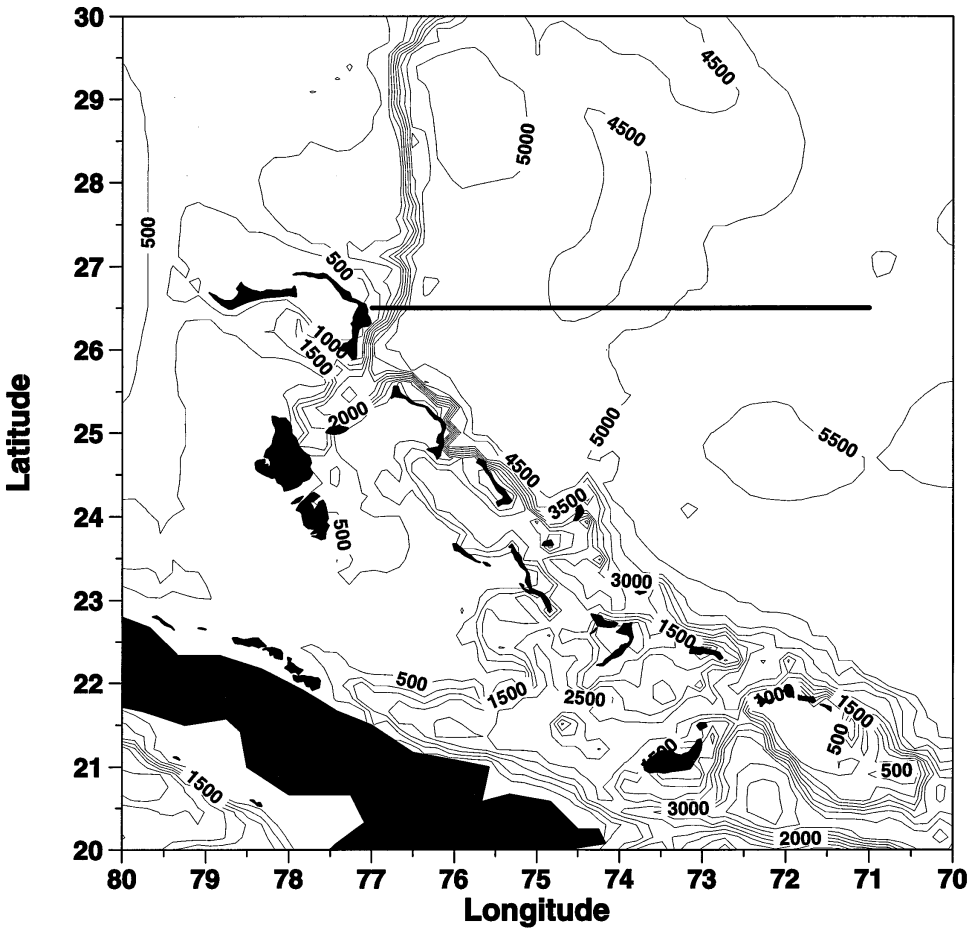

FIG. 1. The Abaco region including bottom topography.

means at each grid point is variable. In particular, no pre-1987 cruises extended offshore beyond 100 km (76°W) (Table 1). Only eight cruises extended out to 200 km and only five out to 300 km. Thus, spatial coverage is most extensive inshore and drops off rapidly east of 100 km.

Time–longitude diagrams were also constructed to portray temporal variability in various layers of the DWBC. A 21 × 21 time–longitude grid was used corresponding to a temporal resolution of about six months and longitude resolution of about 15 km (0.15°).

The properties of four isothermal layers within the DWBC are considered. The layers are based on earlier studies of chlorofluorocarbon (CFC) concentrations in DWBC water masses. The upper layer ($\theta \sim 3.9°$–$5.0°$C) is characterized by a CFC maximum and originates in the southern Labrador Sea (Pickart 1992). Beneath this layer, the temperature range of classical Labrador Sea Water (LSW), 3.2°–3.9°C, is characterized by intermediate CFC concentrations (Fine and Molinari 1988). A minimum CFC layer is bounded by the 2.4° and 3.2°C isotherms and consists mainly of North Atlantic interior water (Fine et al. 1995). Finally, the deepest layer considered (1.85°–2.4°C) is high in CFC concentrations and is primarily Denmark Straits overflow water (Fine 1995).

TABLE 2. Isopycnal and isobaric boundaries between the DWBC layers.

θ	$\sigma_{1.5}$	σ_2	σ_4	$S_{approx.}$	$P_{approx.}$ (dbar)
5.00	34.530	(36.750)		35.050	1200
3.90	34.650	(36.890)		34.990	1600
3.20	34.730	36.975	(45.700)	34.970	2300
2.40		37.055	45.820	34.927	3200
1.85			45.890	34.890	4500

3. Results

a. Average properties

Average sections of potential temperature (θ), salinity (S), and potential density (σ), referenced to 2000 db (σ_2) as functions of pressure, are shown in Figs. 2a–c. The three sections have many similarities. West of about 76°W (100 km) and below 2000 m, the signature of the DWBC in this region, downward sloping of the con-

tours, is evident in all three sections. East of 76°W (100 km) and below 3000 m, the contours slope downward toward the boundary in the three sections. Between 2000 and 3000 m offshore, the contours are nearly horizontal with the suggestion of a weak trough at about 75.5°W (150 km) in the three transects. The isotherms, isohalines, and isopycnals begin sloping upward toward the boundary between 2000 and 1500 m. The salinity section shows a weakened vertical gradient from 1500 to 2000 db (3.5°–4.1°C) across the entire section, at the approximate temperature range of LSW (3.5°–4.1°C). Isohalines, isopycnals, and isobars corresponding to the isotherms that separate the four layers of the DWBC were determined visually from these figures and are summarized in Table 2.

The mean 1984–1993 referenced geostrophic section, estimated as described above, is shown in Fig. 3a. Below 800 m, the maximum mean southward velocity, outlined by the 12 cm s^{-1} isotach, is centered at about 60 km and between 1500 and 2000 db. The core corresponds to a potential temperature range of about 3.3° to 4.5°C (Fig. 3a). The peak southward speed was 15 cm s^{-1}. Weaker southward flow is located between 250 and 300 km (74.5° to 74°W) from roughly 2000 db to the bottom. The southward flows are separated by weak northward flow from about 3000 db to the bottom. Lee et al. (1996) describe a local recirculation gyre using independent data in this region.

Except in the velocity core, the standard deviations (Fig. 3b) are equal to or greater than the means (Fig. 3a). Near the bottom the standard deviations are some three times the mean speeds. Inshore of 100 km, the large standard deviations confirm a conclusion of Leaman and Harris (1990) that the location and intensity of the southward core of the DWBC is fairly variable. Offshore, the larger standard deviations may signify an increased variability or may be a consequence of relatively sparse data distribution.

b. Temporal and spatial variability

Anomalies of θ and S as functions of time and longitude were calculated for the four layers. To eliminate the effects of isopycnal displacements, the layer boundaries are defined by the potential density surfaces given in Table 2. As the salinity variability mimics the temperature variability [i.e., positive (negative) salinity anomalies overlay positive (negative) temperature anomalies], only the temperature variability is described.

In the upper layer, the potential temperature anomalies near the boundary (west of 76°W) are characterized by variability with a timescale of 2–3 yr and .04° to

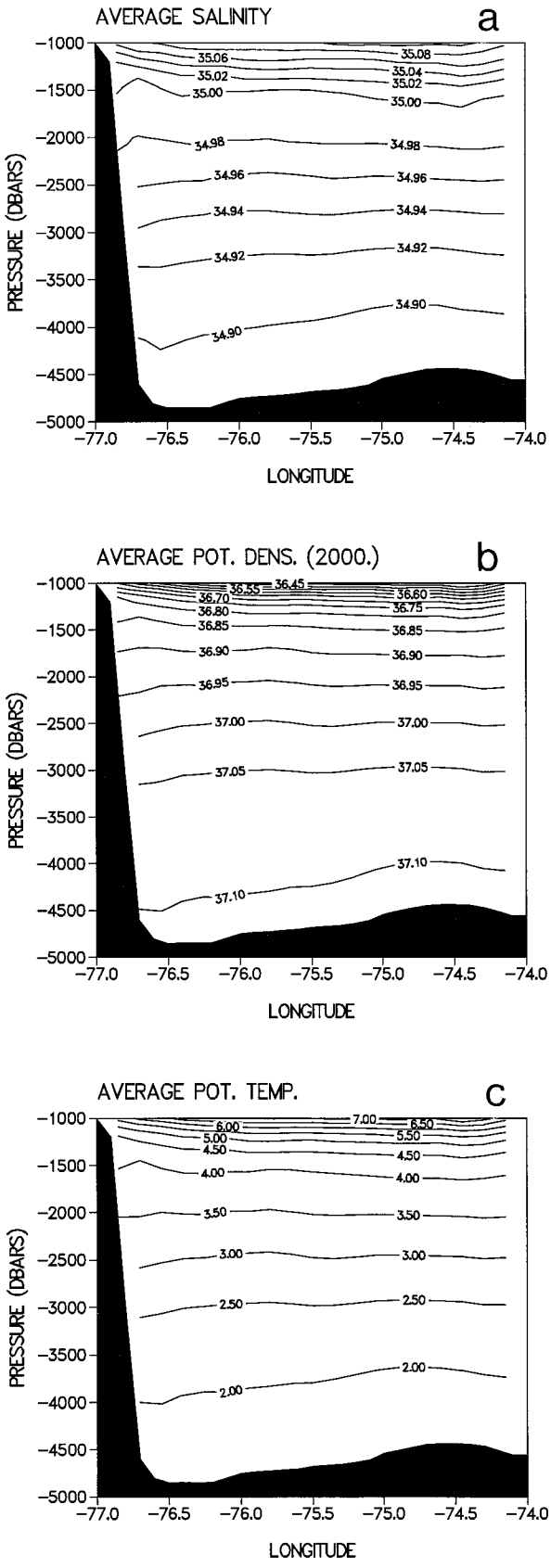

→

FIG. 2. Sections of mean (a) potential temperature, (b) salinity, and (c) potential density (σ_2) for the ten-year period.

.06°C amplitude from the beginning of the record to about 1992 (Fig. 4a). Positive θ anomalies extend to 1993. Offshore, the lack of similar temporal resolution could conceal the 2–3-yr variability. Here positive anomalies also dominate at the end of the record (Fig. 4a).

In the second and third layers, variability is similar with alternating periods of positive and negative anomalies extending from the boundary to offshore (Figs. 4b and 4c). The timescale of the variability is about 4 years and the amplitude is about .03°C in both layers. Periodic variability is not observed in the deepest layer (Fig. 4d), but a transition from negative anomalies at the start of the record to positive anomalies at the end of the record is observed. Maximum temperature anomalies range from about .01° to .02°C.

Current meter observations in the region off Abaco show that the core of the DWBC makes occasional offshore excursions of order 100 km (Lee et al. 1996). These excursions are also apparent in sections of geostrophic velocity (E. Johns et al. 1997, manuscript submitted to *J. Phys. Oceanogr.*). To isolate the water mass characteristics of the velocity core of the DWBC (i.e., the assumed most direct route from the source regions), the stations from the synoptic sections within the geostrophic velocity core were identified (Table 2). Average θ, S, and H values were computed for each occupation of the section. The resulting θ-time series for the four layers are shown in Figs. 5a–d. The error bars in these figures represent the standard errors of the cruise means. Average layer values of θ, S, and H for the entire ten-year period are given in Table 3.

The θ, S, and H time series were fit by a linear equation using a least squares routine. No significant trends were computed for any of the records. The θ-time series (Fig. 5) portray similar variability to that derived from the time–longitude plots (Fig. 4). In the upper layer, variability has about a 2–3-yr period with a .05°C amplitude (Fig. 5a). Amplitudes are smaller in the second and third layers (Figs. 5b and 5c).

To isolate the variability of classical Labrador Sea Water at Abaco, time series of mean properties within the geostrophic velocity core were created for a sublayer of the second layer (Figs. 6a and 6b) defined by $\sigma_{1.5} \sim$ 34.68–34.74 (Talley and McCartney 1982). This layer corresponds to $\theta \sim$ 3.1°–3.65°C and to about 1800–2400 dbar in the Abaco section means (Fig. 2). Minima in potential temperature and salinity for this layer occur in late 1991, and are followed by increases to 1993. The slope of the straight line fits of the entire time series are of the same order as those in the original four layers and are not significant. For comparison with Figs. 6a and 6b, geostrophic core mean properties were calculated for the sublayer of the second layer as defined by the corresponding isobars (1800–2400 dbar) (not shown). Not only is the scale of the variability much larger in the isobaric means, but the temperature and salinity increases and decreases in the isobaric and isopycnal time series are often of the opposite sense. The temperature and salinity increase from 1991 to 1993 and its relevance to the cooling and freshening observed in the central Labrador Sea in the early 1970s (Lazier 1988) will be discussed in more detail later.

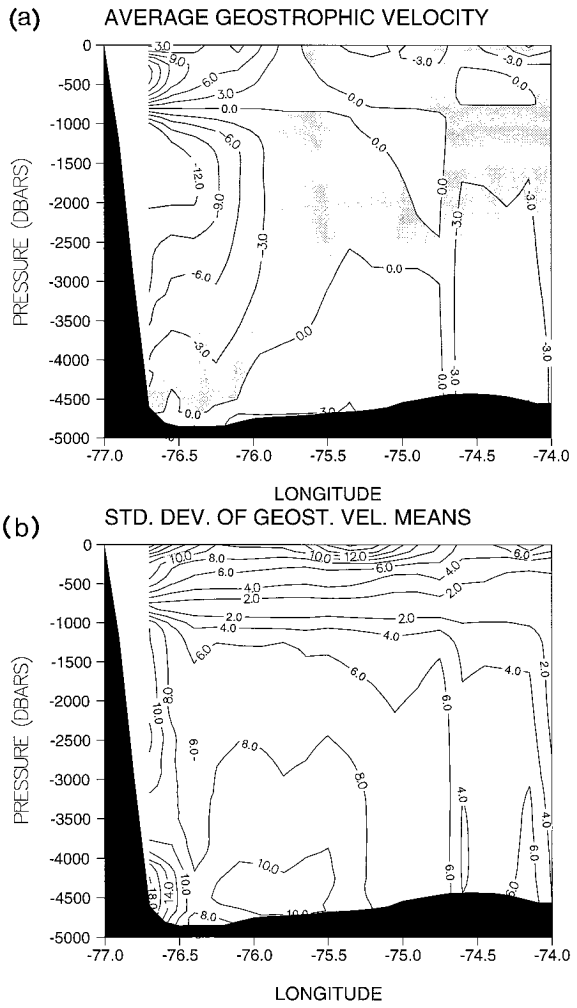

FIG. 3. Sections of (a) mean geostrophic velocity (cm s^{-1}) and (b) standard deviations (cm s^{-1}) of the means for the ten-year period.

4. Section differences

a. Section differencing along isobars and isopycnals

Earlier studies of variability along the 24.5°N transatlantic section computed differences in temperature and salinity along pressure surfaces. These differences can include variability owing to water mass changes, as well as vertical movement of isopycnals. To demonstrate the effect of isopycnal displacements, data from a pair of sections were differenced along both isobars and isopycnals.

The June 1993 and March 1987 sections were differenced because 1) they have the largest temporal spacing for sections that extend to 74°W; 2) the CTD salin-

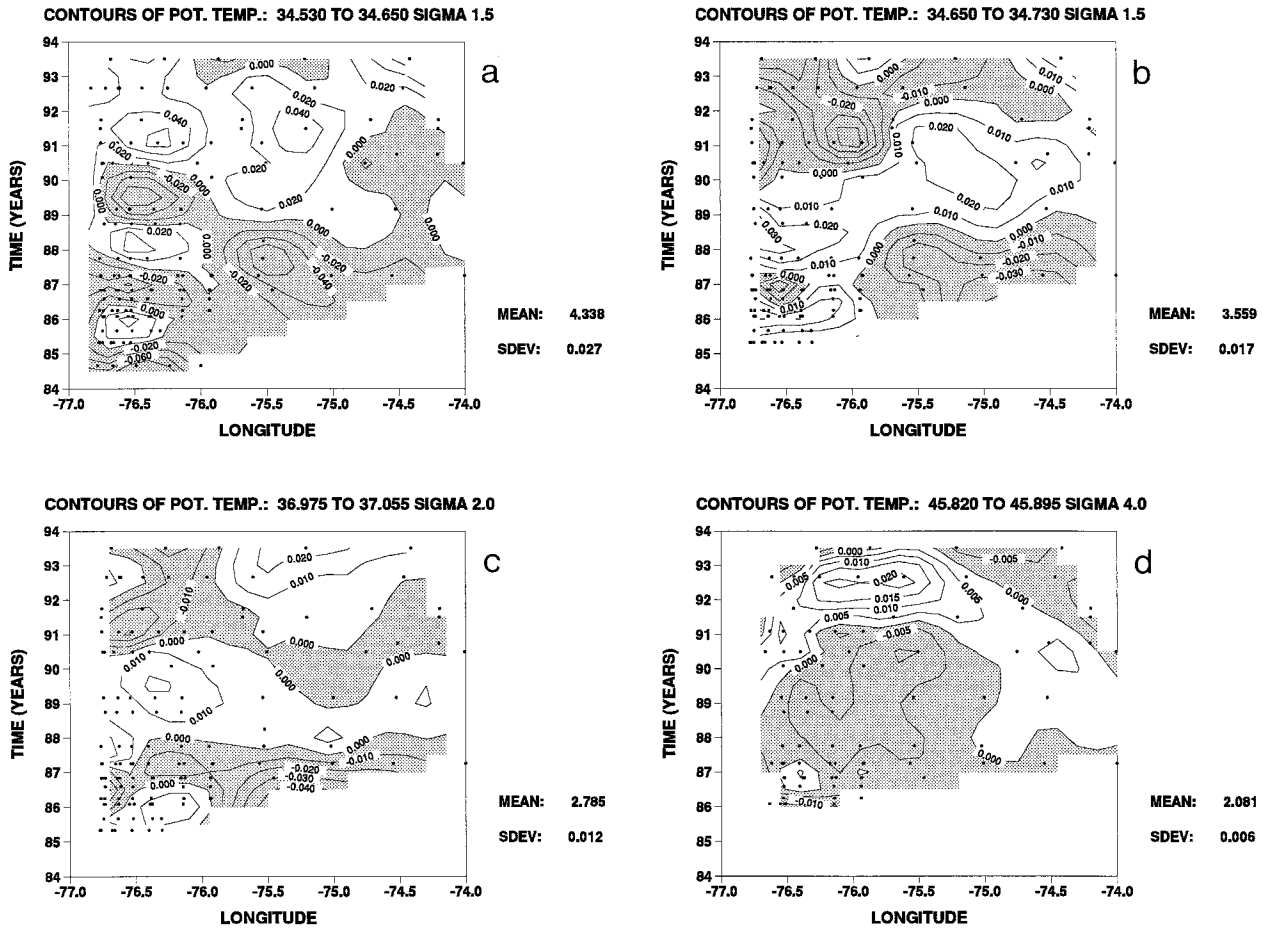

FIG. 4. Time–longitude plots of anomalies of potential temperature for the (a) upper, (b) second, (c) third, and (d) deep layers.

ities were calibrated with in situ samples, not historical data; 3) they exhibit extremes in θ and S anomalies (Fig. 4); and 4) the DWBC velocity core is within 100 km of the boundary during both cruises. In contrast, 1) maximum velocities were greater in 1987 (-25 cm s^{-1}) than in 1993 (-15 cm s^{-1}) and 2) offshore of 100 km, a deep northward flow of $\sim$10 cm s^{-1} appeared in 1987, but not in 1993.

The isobaric temperature difference section (Fig. 7a) is characterized by a cooling ($\sim -.1$°C) in the western part of the section (west of 75.5°W), down to around 3500 dbar, and warming ($\sim .2$°C) to the east. Cooling and warming of this extent and magnitude are not present in the section differenced along isopycnals (Fig. 7d). Similarly, salinity differences are considerably less when computed on isopycnic surfaces (Figs. 7b and 7e). In Fig. 4d, cooling rarely exceeds $-.04$°C, while warming rarely exceeds .08°C. The large disparity between isobaric and isopycnal temperature differences indicates that the variability is primarily due to vertical movement of the isopycnals rather than a true water mass change.

To illustrate the magnitude of the isopycnal movement, a difference section of pressure levels as a function of potential density σ_2 is shown in Fig. 7f. Excursions of ± 100 dbar and larger are present. If the relative expansion of the upper part of the density axis and contraction of the lower part (as compared to pressure) is accounted for, Figs. 7c and 7f appear to share a similar pattern. The apparent warming in the eastern portion of the region was due primarily to a deepening of the isopycnals in June 1993 as compared to March 1987, while the cooling in the western part was due to isopycnal uplifting.

b. Mechanisms responsible for observed differences

Bindoff and McDougall (1994) developed a method for identifying the mechanisms responsible for differences in temperature and salinity characteristics along a section occupied at different times. The method decomposes variability into ''true'' changes in water mass variability and changes due to vertical motions of isotherms and isohalines, with no changes in water mass properties. A simplified version of their analysis was applied to a portion of the Abaco data. First the transects considered in the previous section are analyzed. Then

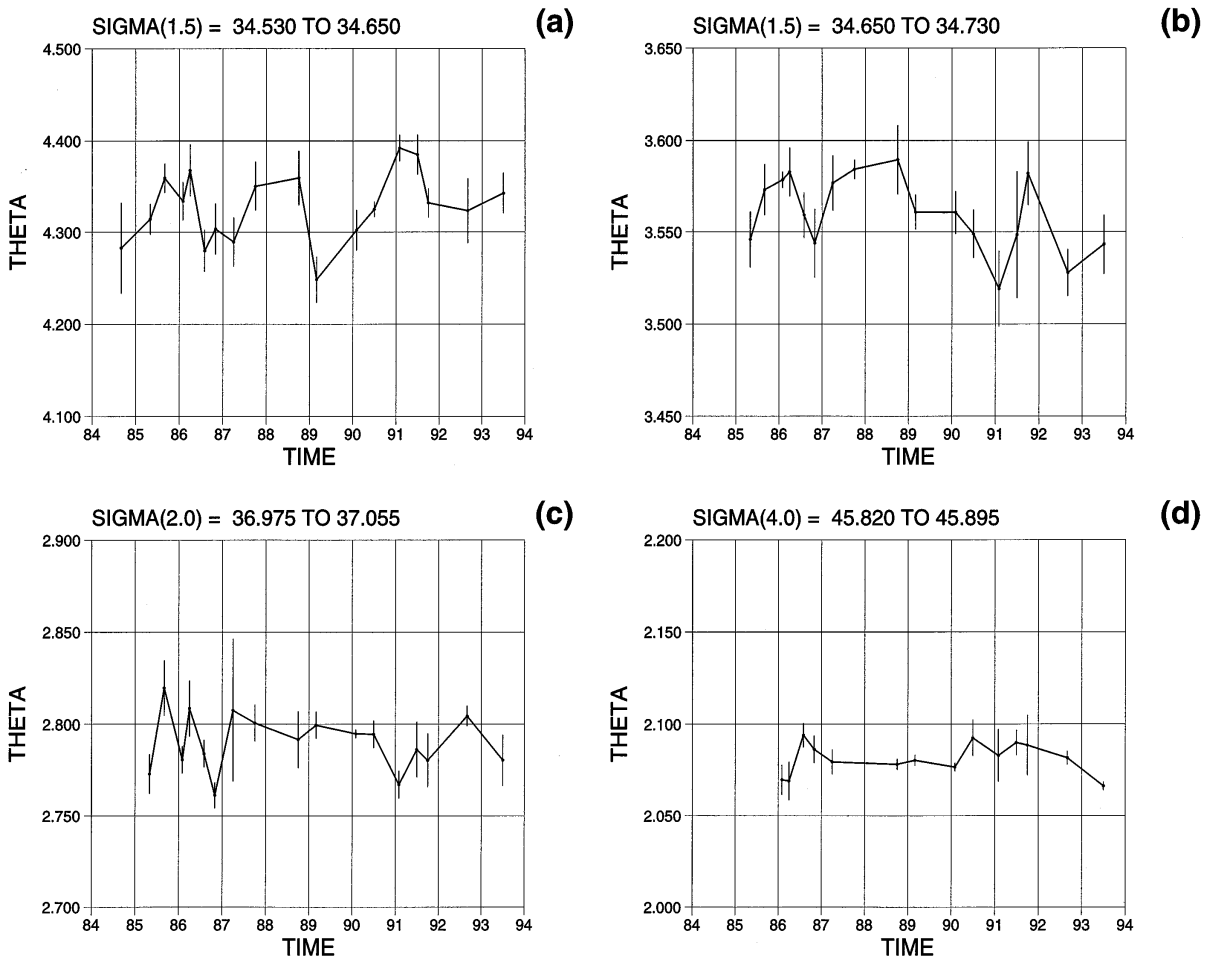

FIG. 5. Time series of mean potential temperature within the geostrophic velocity core for the (a) upper, (b) second, (c) third, and (d) deep layers.

sections that define the 1991 to 1993 variability in LSW (Fig. 6) are considered.

Following Bindoff and McDougall (1994) property differences between two casts on the same section but at different times are defined along isobars and isopycnals (Fig. 8). Bindoff and McDougall (1994) use neutral surfaces in their analysis; referenced isopycnals will be used here. Referenced isopycnals and neutral surfaces are interchangeable as long as the depth range of interest surrounding the isopycnal reference level is small.

TABLE 3. Mean and standard deviations (in parenthesis) for stations within the geostrophic velocity core.

DWBC layer	θ (°C)	S	$\sigma_{1.5;2;4}$	H (dbar)	Number of cruises
Upper	4.33 (.052)	35.014 (.006)	34.605 (.004)	424 (54)	18
Second	3.56 (.031)	34.983 (.003)	34.692 (.003)	695 (115)	17
Third	2.79 (.025)	34.947 (.002)	37.017 (.003)	803 (74)	17
Deep	2.08 (.014)	34.908 (.001)	45.869 (.002)	1319 (116)	14

The property ($\psi = \theta$ or S) differences along isobars are given by

$$\psi'|_z = \psi_c - \psi_a$$

and differences along isopycnals by

$$\psi'|_n = \psi_b - \psi_a,$$

where $\psi = \theta$ or S. The difference between $\psi'|_z$ and $\psi'|_n$ from the diagram,

$$\psi'|_z - \psi'|_n = \psi_c - \psi_b = N'\psi_z,$$

is equal to the pressure level change of the isopycnal (N') times the vertical gradient of ψ (ψ_z). Following Bindoff and McDougall's convention, N' is considered greater than zero when the isopycnal surface rises. Multiplying the potential temperature equation by the thermal expansion coefficient α and the salinity equation by β, the salinity contraction coefficient, yields

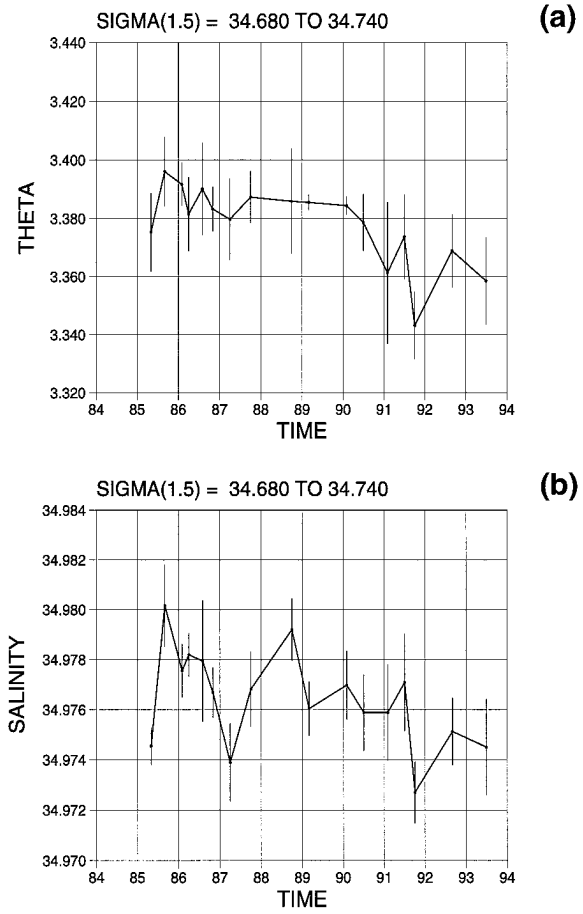

FIG. 6. Time series of mean (a) potential temperature and (b) salinity within the geostrophic velocity core for a sublayer of the second layer defined by $\sigma_{1.5}$ = 34.680–34.740.

$$\alpha\theta'|_z = \alpha\theta'|_n - \alpha N'\theta|_z \quad (1)$$

and

$$\beta S'|_z = \beta S'|_n - \beta N' S_z. \quad (2)$$

Bindoff and McDougall (1994) define a stability ratio R_ρ,

$$\alpha\theta_z = R_\rho \beta S_z, \quad (3)$$

and note also that along isopycnals

$$\alpha\theta'|_n = \beta S'|_n. \quad (4)$$

Four variables, $\alpha\theta'|_z$, $\alpha\theta'|_n$, $\beta S'|_z$, and $\beta S'|_n$, are simply changes in θ and S along isobars (z) and isopycnals (n) and two variables, $\alpha N'\theta_z$ and $\beta N' S_z$, are the vertical gradients of θ and S times the vertical displacements of the isopycnals. All variables are dimensionless.

Bindoff and McDougall (1994) identify three ''pure'' mechanisms to describe the temperature and salinity changes between two repeat hydrographic sections. A change caused only by vertical motion of the isopycnals is called pure heave. Differences resulting from the modification of a particular water mass (warming with no corresponding change in salinity or freshening with no corresponding change in temperature), and the subduction of the water mass is called pure warming or pure freshening. Pure heave is caused by changes along isobars, not along isopycnals. Pure warming and pure freshening are characterized by changes along both isopycnals and isobars.

Bindoff and McDougall (1994) use their theoretical arguments about average θ or S changes for pure warming, pure freshening, and pure heave to derive relationships between the six variables [Eqs. (1)–(4)] for each of the three processes. These relationships are summarized below. Some expressions are clear from the θ–S diagram as shown in Fig. 9, others are derived from Eqs. (1)–(4).

For pure warming,

$$\alpha\theta'|_z > 0$$

$$\beta S'|_z = 0$$

$$\beta S'|_n = N'\beta S_z = \alpha\theta'|_n = -\alpha\theta'|_z (R_\rho - 1)^{-1}.$$

Pure freshening:

$$\alpha\theta'|_z = 0$$

$$\beta S'|_z < 0$$

$$\alpha\theta'|_n = N'\alpha\theta_z = \beta S'|_n = \beta S'|_z (1 - R_\rho^{-1})^{-1}$$

Pure heave:

$$\alpha\theta'|_n = 0$$

$$\beta S'|_n = 0$$

$$\beta S'|_z = -N'\beta S_z$$

$$\alpha\theta'|_z = -N'\alpha\theta_z.$$

Schematic illustrations of these relationships for the case of $R_\rho > 1$ are shown in Figs. 10a–c. The slopes of the vectors representing each process are defined by the above equations. Each data point represents some linear combination of the three processes (warming, freshening, or heave). A dominant process is identified by a clustering of points along its theoretical vector. The axes were chosen so that two processes were orthogonal and the third was a unit diagonal. The axes in the third plot (Fig. 10c) were obtained by rearranging the last two equations for pure heave above.

Bindoff and McDougall (1994) applied their method to repeat sections in the Tasman Sea. The casts in each Tasman Sea section were averaged into a single ''cast,'' so the potential temperature and salinity difference terms were calculated from two average casts. In the Abaco analysis, the data for each cruise were interpolated onto gridded sections. The difference terms were calculated at each grid point.

The Abaco data from repeat sections between 77° and 74°W in June 1993 and March 1987 were interpolated onto 21 × 61 elements grids as described earlier. The

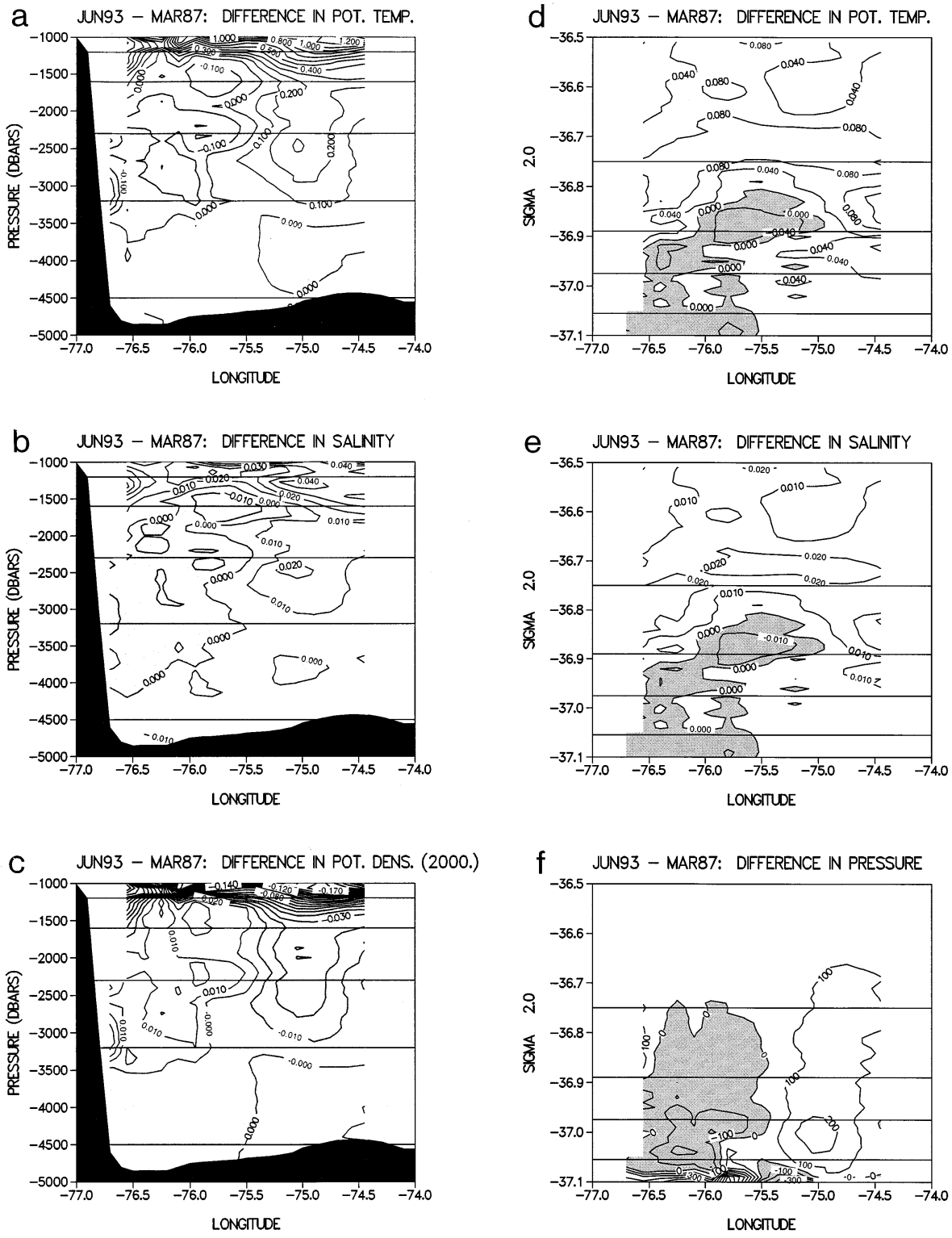

FIG. 7. Section differences between June 1993 and March 1987 of potential temperature, salinity, and potential density (σ_2) along isobars (a, b, c) and along isopycnals (d, e, f). The potential density and pressure levels bounding the four DWBC layers (Table 2) are highlighted.

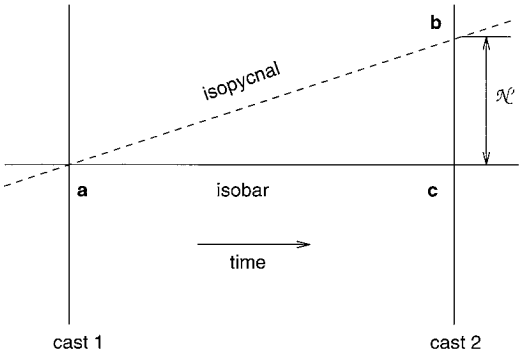

FIG. 8. Definitions of the isopycnal and isobaric difference terms (adapted from Bindoff and McDougall 1994, their Fig. 5).

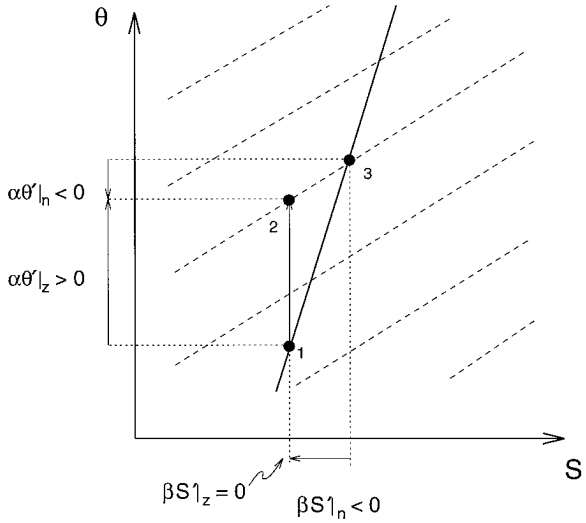

FIG. 9. The pure warming process. The mean temperature of a layer (''1'') warms to ''2'' with no change in salinity. The new water mass (''2'') appears cooler and fresher than the original water mass (solid line) on the same isopycnal (''3'') (adapted from Bindoff and McDougall 1994, their Fig. 1).

sections were subtracted along both isobars and isopycnals to form the six difference terms. Initial plots of the entire section, representing a combination of the DWBC and the surrounding water masses, were inconclusive. To isolate the DWBC characteristics, the differences for each grid element inshore of 75.5°W were plotted as individual points on the axis pairs shown in Fig. 10 for each of the four layers. All axes were scaled by 10^{-5}. Results for the upper, second, third, and deep layers are shown in Figs. 11a–d. For all layers, $R_\rho \approx 4$.

Comparison of Fig. 11a with the theoretical plots (Fig. 10b) shows that the variability from 1987 to 1993, in the upper layer, thought to originate in the southern Labrador Sea, was mostly due to pure salinification. Note that the magnitude of the salinification at the source (''1'' to ''2'' in Fig. 9) cannot be estimated from Fig. 11a. The slight upward displacement of the predominantly diagonal distribution in Fig. 11a suggests that water in this layer may have been subjected to some cooling as well.

In the second layer, thought to consist mainly of classical LSW, some indication of all three processes are present. Figure 11b suggests that variability in this layer from 1987 to 1993 may have been due to pure cooling, although the indication is weak. Some parts of the layer show signs of salinification.

Most of the variability in the third and deep layers (Figs. 11c and 11d) is due to pure heave. In the third layer, positive heave (isopycnal uplifting) is the dominant process (Fig. 11c). Some suggestion that the layer may have been subjected to a weak cooling process (downward displacement in Fig. 11c) is also present. In the deep layer, negative heave (isopycnal deepening) is the dominant process (Fig. 11d).

The relationships between the difference variables ($\theta'|_n$ $\theta'|_z$, etc.) for each dominant process are verified by the section difference plots (Fig. 7) inshore of 75.5°W. From the θ–S diagram for pure freshening (Fig. 2 from Bindoff and McDougall 1994) and the theoretical relationships in section 4b, the pure salinification process is characterized by negligible heave ($N' \sim 0$), increased potential temperature and salinity along isopycnals ($\theta'|_n > 0$, $S'|_n > 0$), increased salinity along isobars ($S'|_z > 0$), and negligible potential temperature change along isobars ($\theta'|_z \sim 0$). In the upper layer (above 36.89 σ_2) and inshore of 75.5°W in Fig. 7f, the change in pressure ($P'|_n$) is approximately zero. Note that for $P'|_n < 0$, $N' > 0$ and for $P'|_n > 0$, $N' < 0$. Above 36.89 and inshore of 75.5°W in Figs. 7d and 7e, $\theta'|_n > 0$ and

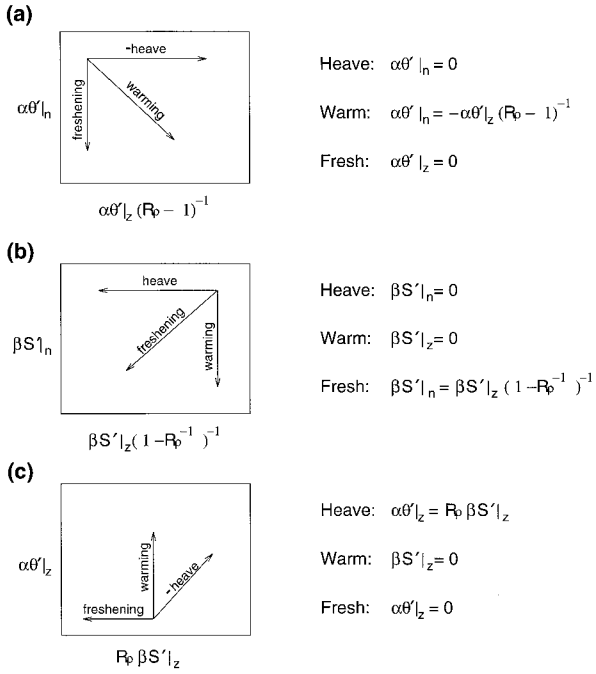

FIG. 10. Schematic illustrations of the theoretical relationships for pure warming, pure freshening, and pure heave.

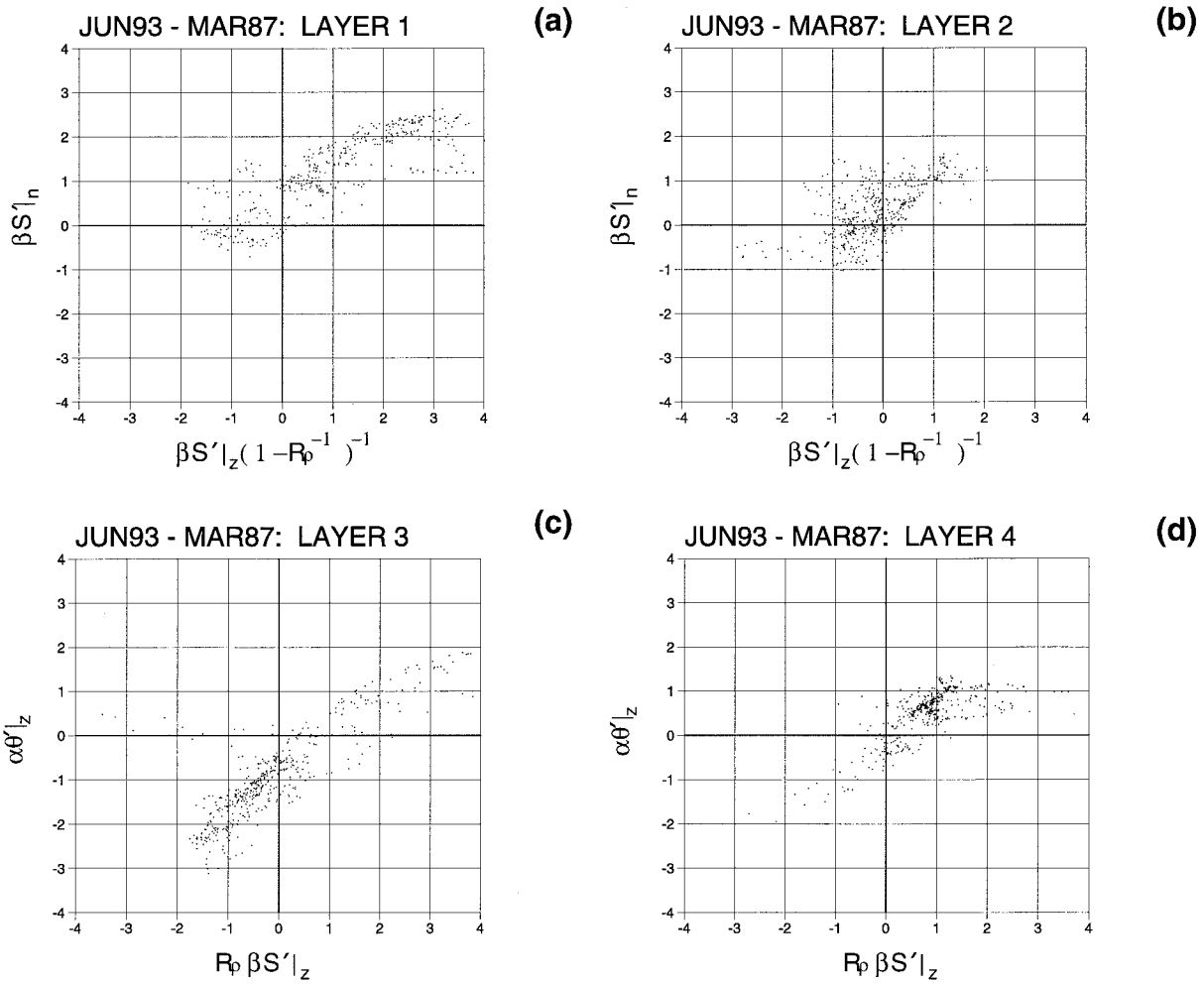

FIG. 11. Scatterplots of the Abaco data representing differences from March 1987 to June 1993 for the (a) upper, (b) second, (c) third, and (d) deep layers.

$S'|_n > 0$. In this same region, above 1600 dbar and inshore of 75.5°W from Fig. 7b, $S'|_z > 0$. From Fig. 7a, some warming and cooling is also present. ''Heave'' in the deepest two layers may be verified similarly from Fig. 7f.

The time series of geostrophic velocity core mean properties in section 3b for the layer $\sigma_{1.5} = 34.680$–34.740 (classical LSW) showed an increase in θ and S from late 1991 to mid-1993 (Figs. 6a and 6b). To determine the cause of this observed variability, scatterplots of the type in Fig. 11 were created for this layer over the period September 1991 to June 1993. Even though the layer was observed to have warmed and salinified, Fig. 12 clearly identifies ''pure cooling'' as the dominant water mass modification (see Fig. 10a) responsible for the observed variability.

5. Discussion

Earlier studies of changes in the temperature and salinity structure of the subtropical Atlantic were typically based on transatlantic sections widely spaced in time. For example, P94 described 1981 and 1992 transects. The ten-year time series of hydrographic data from the Abaco section provides temporal resolution not available to P94. However, differences in data and analysis techniques must be considered to establish the limitations of comparisons between the P94 and our study.

The P94 section traversed the basin at 24.5°N, our section is limited to the western Atlantic at 26.5°N (Fig. 1). P94 smoothed their sections by applying a horizontal Gaussian filter 300 km in width. The entire Abaco section is only 300 km wide and no filtering was applied. Further, P94 assumed zero temperature difference at the boundary, which was propagated offshore by the Gaussian filter. P94 acknowledge that their method eliminates small-scale features and reduces differences near the boundary. The Abaco section captures small-scale boundary features.

Near the western boundary, P94 reported cooling between 1981 and 1992 of about .05°C from 1500 to 2200 m, warming of .025°C from 2300 to 2600 m, and cooling

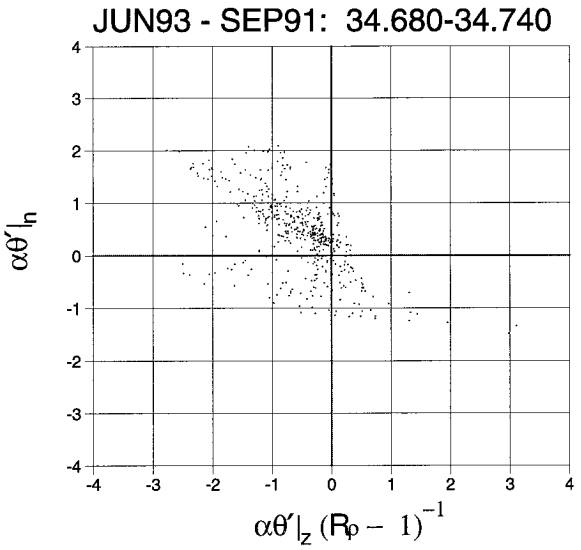

FIG. 12. Scatterplot for a sublayer of the second layer defined by $\sigma_{1.5}$ = 34.680–34.740 representing differences from September 1991 to June 1993.

of .025°C from 2600 m to the bottom. Isobaric temperature differences between 1987 and 1993 indicate cooling of about .1°C over the western portion of the section and warming of about .2°C over the eastern portion (Fig. 7a). However, the time–longitude plots in Fig. 4 indicate that particularly close to the boundary the variability between 1987 and 1993 is not necessarily a long-term warming trend but phases of a quasiperiodic signal. Time series of mean properties of each layer within the geostrophic velocity core (Fig. 5) are consistent with the time–longitude plots. Additional data are required to determine if these nearshore signals are representative of offshore conditions (i.e., offshore, are P94 results representative of a long-term trend or higher frequency variability as near the boundary).

Displaying differences by pressure and potential density (Fig. 7) and applying the analysis technique of Bindoff and McDougall (1994) to the 1987 and 1993 sections permits definition of the mechanisms responsible for the observed changes. The increased magnitudes of the temperature and salinity changes resulting from the inclusion of vertical displacements in the isobaric differences is apparent (Fig. 7). Previous investigators (Roemmich and Wunsch 1984; P94) have drawn conclusions about basin-scale warming and cooling in the Atlantic using isobaric section differences. The Bindoff and McDougall (1994) method allows further decomposition of the observed changes into those caused by vertical displacements of isotherms and isohalines versus changes in water mass characteristics.

The utility of Bindoff and McDougall (1994) was exemplified by applying the method to a sublayer of the second layer defined by $\sigma_{1.5}$ = 34.68 to 34.74 ($\theta \sim 3.1$ to 3.6). The sublayer, created to isolate the variability of classical LSW, showed an increase in potential temperature and salinity from 1991 to 1993 (Figs. 6a and 6b). The scatterplot in Fig. 12 identified pure cooling as the dominant mechanism responsible for the changes. The possibility that this cooling originated in central Labrador Sea and was advected southward is now explored.

A time series showing the mean θ and S variability of classical LSW over the past three decades (Read and Gould 1992) is available for comparison with the Abaco data. From 1962 to 1971 convection in the central Labrador Sea was diminished, and at its source the temperature and salinity of LSW increased (Talley and McCartney 1982; Read and Gould 1992). From 1971 to 1976 and from 1984 to 1990 and afterwards, deep convection was present and LSW cooled and freshened by as much as .6°C and .06 in salinity. Minimum temperatures occurred in 1976 and 1993, although the 1976 minimum may be overestimated (J. Lazier 1995, personal communication). Unlike most years, the data in 1976 were collected in winter during a deep convection event. The temperature and salinity would probably have been greater if the measurements were taken later in the year, like most of the other values. The decrease in temperature and salinity in the early 1970s, indicating a period of increased deep water renewal, is more suitable for time series comparisons (J. Lazier 1995, personal communication).

Based on CFC measurements, Fine (1995) estimated the timescale for the advection of deep water from the southern Labrador Sea ventilation region to the Abaco section to be about 18 years. If the warming and salinification at Abaco from 1991 to 1993 was caused by a cooling of the central Labrador Sea convective mixed layer, the cooling would have had to occur from about 1973 to 1975, assuming an advective timescale of 18 years. Assuming an advection time of 20 years corresponds to a production time from 1971 to 1973. Both estimates are within the period of active renewal in the Labrador Sea. Recognizing the uncertainties associated with estimating advective timescales based on CFC measurements and given that there are no sources of cooler, fresher water south of the Labrador Sea, it is plausible that the pure cooling of the water parcels comprising the $\sigma_{1.5}$ = 34.68 to 34.74 sublayer, which resulted in the observed θ and S increases from 1991 to 1993, occurred in the central Labrador Sea in the early 1970s.

Acknowledgments. Numerous helpful discussions with Tom Lee, Elizabeth Johns, Trevor McDougall, and Rana Fine are gratefully acknowledged. This research was carried out under the auspices of the Cooperative Institute for Marine and Atmospheric Studies, a Joint Institute of the University of Miami and the National Oceanic and Atmospheric Administration, through Cooperative Agreement NA37RJ0200.

REFERENCES

Bindoff, N. L., and T. J. McDougall, 1994: Diagnosing climate change and ocean ventilation using hydrographic data. *J. Phys. Oceanogr.,* **24,** 1137–1152.

Fine, R. A., 1995: Tracers, time series and the thermohaline circulation: The lower limb in the North Atlantic Ocean. *Rev. Geophys.,* **33** (suppl.), 1353–1365.

——, and R. L. Molinari, 1988: A continuous deep western boundary current between Abaco (26.5°N) and Barbados (13°N). *Deep-Sea Res.,* **35,** 1441–1450.

Johns, E., and A.-M. Wilburn, 1993a: Hydrographic observations in the western tropical and subtropical North Atlantic Ocean: ACCP and WESTRAX during 1990. NOAA Data Rep. ERL AOML-22, 103 pp. [Available from NOAA/AOML, 4301 Rickenbacker Causeway, Miami, FL 33149.]

——, and ——, 1993b: Hydrographic observations in the western tropical and subtropical North Atlantic Ocean: ACCP and WESTRAX during 1991. NOAA Data Rep. ERL AOML-23, 82 pp. [Available from NOAA/AOML, 4301 Rickenbacker Causeway, Miami, FL 33149.]

——, R. A. Fine, and R. L. Molinari, 1996: Recirculation of the deep western boundary current south of the Blake Bahama outer ridge. *J. Phys. Oceanogr.*,

Lazier, J. R. N., 1988: Temperature and salinity changes in the deep Labrador Sea, 1962–1986. *Deep-Sea Res.,* **35,** 1247–1253.

Leaman, K. D., and J. E. Harris, 1990: On the average absolute transport of the deep western boundary current east of Abaco Island, the Bahamas. *J. Phys. Oceanogr.,* **20,** 467–475.

Lee, T. N., W. Johns, F. Schott, and R. Zantopp, 1990: Western boundary current structure and variability east of Abaco, Bahamas, at 26.5°N. *J. Phys. Oceanogr.,* **20,** 446–466.

——, ——, R. J. Zantopp, and E. R. Fillenbaum, 1996: Moored observations of western boundary current variability and thermohaline circulation at 26.5°N in the subtropical North Atlantic. *J. Phys. Oceanogr.,* **26,** 962–983.

McCartney, M. S., 1992: Recirculating components to the deep boundary current of the northern North Atlantic. *Progress in Oceanography,* Vol. 29, Pergamonn, 283–383.

Molinari, R. L., R. A. Fine, and E. Johns, 1992: The deep western boundary current in the tropical North Atlantic Ocean. *Deep-Sea Res.,* **39,** 1967–1984.

Parrilla, G., A. Lavin, H. Bryden, M. Garcia, and R. Millard, 1994: Rising temperatures in the subtropical North Atlantic Ocean over the past 35 years. *Nature,* **369,** 48–51.

Pickart, R. S., N. G. Hogg, and W. M. Smethie, 1989: Determining the strength of the deep western boundary current using the chlorofluoromethane ratio. *J. Phys. Oceanogr.,* **19,** 940–951.

Read, J. F., and W. J. Gould, 1992: Cooling and freshening of the subpolar North Atlantic Ocean since the 1960s. *Nature,* **360,** 55–57.

Roemmich, D., and C. Wunsch, 1984: Apparent changes in the climate state of the deep North Atlantic Ocean. *Nature,* **307,** 447–450.

Rosenfeld, L. K., R. L. Molinari, and K. D. Leaman, 1989: Observed and modeled annual cycle of transport in the Straits of Florida and east of Abaco Island, the Bahamas (26.5°N). *J. Geophys. Res.,* **94** (C4), 4867–4878.

Talley, L., and M. S. McCartney, 1982: Distribution and circulation of Labrador Sea Water. *J. Phys. Oceanogr.,* **12,** 1189–1205.

Wilburn, A.-M., E. Johns, and M. H. Bushnell, 1987: Current velocity and hydrographic observations in the Straits of Florida, the Caribbean Sea, and offshore of the Antillean Archipelago: STACS 1986. NOAA Data Rep. ERL AOML-10, 247 pp. [Available from NOAA/AOML, 4301 Rickenbacker Causeway, Miami, FL 33149.]

——, ——, and ——, 1988: Current velocity and hydrographic observations in the southwestern North Atlantic Ocean: STACS 1987. NOAA Data Rep. ERL AOML-12, 86 pp. [Available from NOAA/AOML, 4301 Rickenbacker Causeway, Miami, FL 33149.]

——, ——, and ——, 1989: Current velocity and hydrographic observations in the southwestern North Atlantic: STACS 1988. NOAA Data Rep. ERL AOML-13, 83 pp. [Available from NOAA/AOML, 4301 Rickenbacker Causeway, Miami, FL 33149.]